Journal of Statistical Physics, Vol. 33, No. 2, 1983

Stochastic Dynamics of the Cubic Map: A Study of Noise-Induced Transition Phenomena

Simon Fraser, Edward Celarier, and Raymond Kapral[1,2]

Received February 23, 1983

The effects of finite-amplitude, additive noise on the dynamics generated by a one-dimensional, two-parameter cubic map are considered. The underlying deterministic system exhibits bistability and hysteresis, and noise-induced processes associated with these phenomena are studied. If a bounded noise source is applied to this system, trajectories may be confined to a finite region. Mechanisms are given for the merging transitions between different parts of this region and the eventual escape from it as the noise level is increased. The noisy dynamics is also represented by an integral evolution operator, with an equilibrium density function with finite support. The operator's spectrum is determined as a function of map parameters and noise amplitude. Such noisy one-dimensional maps can provide models for the study of noise-induced phenomena described by stochastic differential equations.

KEY WORDS: Nonlinear stochastic difference equation; integral master equation; noise-induced transition.

1. INTRODUCTION

It is well known that external noise or fluctuations can have important effects on the dynamics of nonlinear, dissipative systems near bifurcation: noise may promote the existence of new states or enhance the stability of existing states. The spectral density of the noise perturbing the system is also important: in hydrodynamics, finite-power noise may imitate the effects of higher modes on those that govern the system's evolution; in biology and physiology, oscillators are always susceptible to slowly varying random influences, e.g., mild perturbation of the normal (periodic) sinus

[1] Department of Chemistry, University of Toronto, Toronto, Ontario, M5S 1A1, Canada.
[2] On sabbatical leave at Service de Chimie Physique II, Universite Libre Bruxelles, 1982–1983.

0022-4715/83/1100-0341$03.00/0

rhythm of the heart. The fact that such phenomena occur widely and have physical relevance has stimulated much recent activity on this problem.[3]

Nonlinear differential flows exist frequently as (underlying) models of these continuous, physical systems. Next amplitude maps derived from the Poincaré surfaces of section of such flows provide exact, simplified, discrete-time descriptions of their evolution.[2] For strongly dissipative flows, even reduction to a one-dimensional map preserves important characteristics of the flow geometry and the more conspicuous features of the parameter-space phase diagram of structurally stable flow behavior. For example, the period-three bistability and hysteresis phenomena of the Rössler flow[3] can be discussed in terms of the corresponding phenomena in a model cubic map.[4] Here the bistability arises from dynamical effects, rather than from the system potential. There have also been a number of other studies of one-dimensional maps which exhibit bistability.[5–7] Since one-dimensional maps can imitate strongly dissipative flows, it is clearly of interest to examine the effects of noise on the dynamics of these discrete-time systems.[8–11] Most studies to date have been on the logistic model,[9–11] with Gaussian or amplitude-limited (rectangular) noise. In this context, maps with rectangular noise are the discrete paradigm of flows in the presence of finite-power fluctuations. As shown by Mayer-Kress and Haken,[10] finite-amplitude noise allows one to establish sharp criteria for transitions between orbit components; similar abrupt changes occur in the spectrum of the integral evolution operator for the system.

The present work is devoted to a study of noise-induced phenomena that occur for (a dynamical system defined by) a particular cubic map. Our primary goal is to characterize the escape and confinement criteria in the period-one and period-two regimes of the parameter space, along with the associated spectral properties of the evolution operator for the case of an amplitude-limited noise source. Although we only treat the period-one and -two regimes, even here the phenomena are rich and varied.

The outline of the paper is as follows. In Section 2 we present a summary of those aspects of the two-parameter cubic map which are relevant to our studies of noise-induced phenomena. Since bounded noise permits the existence of noisy states with finite support, one may discuss the mechanisms by which, for example, two noisy orbits coalesce to form a single noisy orbit, or escape from a finite interval occurs. In Section 3 we characterize such mechanisms and give conditions for the sharp transitions that take place. The fourth section is devoted to a study of the noisy dynamics from the point of view of the integral (Chapman–Kolmogorov) equation. Here the focus is on the spectral properties of the integral

[3] See, for instance, Ref. 1.

operator, and we examine the structure of the eigenvalue spectrum, and the associated eigenvectors, as a function of the map parameters and noise amplitude. The final section contains a discussion of our findings, along with some comments on the relevance of these noisy map models to noisy differential flows. In addition, we briefly contrast the amplitude-limited noise case with that of an unbounded noise source.

The present work should provide a basis for further studies of noise-induced processes involving oscillating, bistable stages, and hysteresis effects since these phenomena are amenable to a description in terms of a one-dimensional map. Such coexistence of oscillating states has been observed in a number of (differential equation) models,[4–12] as well as experimentally.[6]

2. THE DETERMINISTIC CUBIC MAP

In this section we consider the discrete dynamical system defined by

$$x_{t+1} = C(x_t; a, b) \tag{2.1}$$

where C is the cubic polynomial

$$C(x; a, b) = ax^3 + (1 - a)x + b(1 - x^2) \tag{2.2}$$

The regions in which certain characteristic behaviors are observed are displayed in Figs. 1a and 1b. We shall consider the effects of noise on the dynamical system in this portion of the phase diagram. The parametric form of the map in Eq. (2.2) makes this phase diagram symmetric about the line $b = 0$, since trajectories $\{x_t\}$ at (a, b) have mates $\{-x_t\}$ at $(a, -b)$.

Some aspects of this and related phase diagrams have been described previously,[4,13–17],[4] so we restrict our description to those features which are relevant to the present study. Beyond the rather large region of stable period-one (contained between the boundaries t and h in Fig. 1a) there is a region where more subtle dynamics occurs. On h (whose equation is $b^2 + a(2 - a) = 0$) period one subharmonically bifurcates to period two. At $b = 0$, $a = 2$, the period-two orbit is born symmetrically out of the origin $x = 0$, but it is born unsymmetrically elsewhere on h. Along $b = 0$ the symmetric orbit becomes doubly superstable at the lower crossing of the dashed lines (Fig. 1a) and then undergoes a symmetry breaking bifurcation at $a = 3$ in which two period-two orbits are produced by an orbit doubling process at the cusp of t' (Fig. 1b). Although these new orbits are not symmetric even for $b = 0$, taken together, they possess the symmetry of the map. Elsewhere on t' one period-two is produced by a tangent process[2]

[4] For a discussion of the antisymmetric cubic map, $b = 0$, see Ref. 14. Some of the features described here have been shown to exist in the map $x_{t+1} = x_t + a + b \sin^2 \pi x_t$ in Ref. 17.

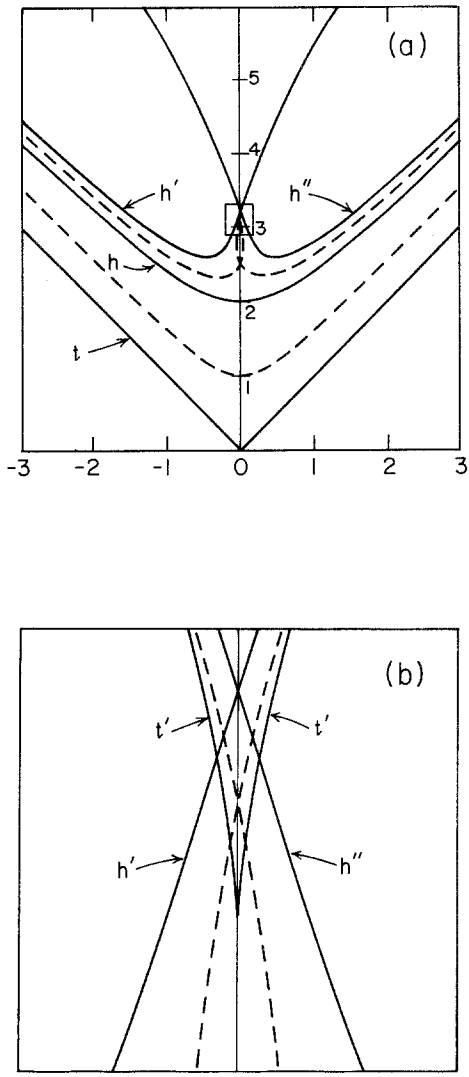

Fig. 1. (a) Phase diagram for the cubic map in the (a, b) plane showing the period-one and period-two regions: t denotes the tangent boundary where period-one is first born; h is the harmonic boundary where bifurcation from period-one to period-two takes place; h' and h'' are harmonic boundaries separating period-two and period-four. The inner dashed lines are lines of superstability for period-one and period-two orbits. An enlarged view of the small square is shown in Fig. 1b. (b) An enlarged view of the region where the h' and h'' boundaries cross. The inner tangent boundary t' is also shown. This boundary denotes the bifurcation from a single period-two orbit to two distinct period-two orbits: inside this boundary hysteresis and bistability occur.

and the other is a continuation of the existing period-two. Bistability exists inside the cusp region enclosed by t' and hysteresis phenomena are possible. As discussed earlier[4] a cusp catastrophe manifold in $\{x\}X\{a,b\}$ is the fixed point solution set which underlies the dynamical effects. Everywhere within the cusp region, three period-two solutions exist: the inner sheet of the catastrophe manifold is the unstable period-two solution.

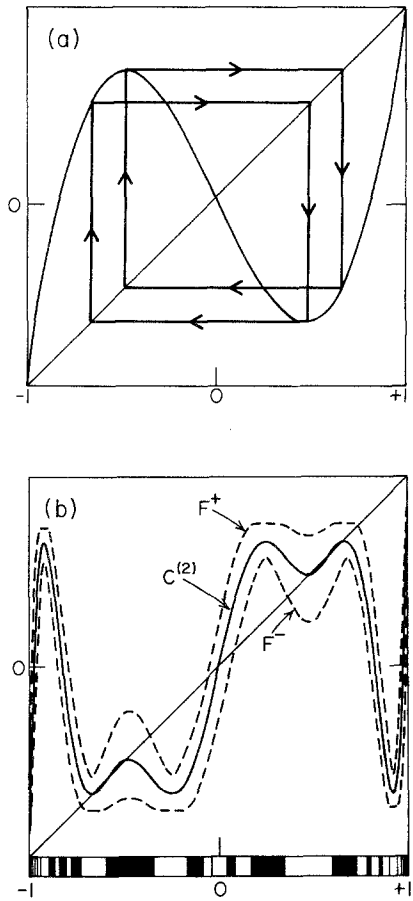

Fig. 2. (a) Sketch of the cubic map for $a = 3.1$ and $b = 0.0$ showing the two coexisting period two orbits. (b) The second power of the cubic map, $C^{(2)}(x; a, b)$ (central solid curve), for the same parameters as in (a). The heavily shaded regions at the base of the figure denote the basin associated with one of the period-two orbits, while the unshaded regions refer to the basin of the other period-two orbit. The dashed curves in this figure are the NL second power functions, $F^{\pm}$, discussed in Section 3 for $\beta = 0.075$.

The crossing of the superstable lines within t' implies that two distinct superstable period-two orbits exist, one belonging to each map extremum. An example of two coexisting period-two orbits is shown in Fig. 2a.

In the regions of parameter space where single periodic motion exists, the basin of the stable attractor is the entire interval $I = [-1, 1]$. However, in the bistable region, the interval I splits into complementary interleaved basins.[18] Throughout the cusp region there is a denumerable infinity of preimages of the unstable period-two fixed points which separate the basin components for the two stable period-two attractors. For $b = 0$ the fragments of each basin cluster at -1, 0, and 1 in I. By symmetry, for $b = 0$, the measure of each basin must be half that of I. In contrast, for $b \neq 0$, one stable period-two orbit exists on both sides of t' while the stable-unstable pair, since they arise by a tangent process, exist only on the inside of t'. As a result, the fixed points of the stable and unstable period-two orbits (and their preimages) are always close to each other near t', though relatively far from the coexisting period-two; thus the measure of the basin of the newly born attractor grows as $\epsilon^{1/2}$, where ϵ is the distance from t', since the second-power map is locally quadratic near the tangent point. Only at the cusp do the basin measures change discontinuously. The basin structure for period-two at $a = 3.1$, $b = 0$ is shown in Fig. 2b; the second power of the map is also displayed. The fragmented basin structure could have important implications for certain types of noise-induced processes.

In this paper we discuss the dynamics for period-one and -two and hysteresis in the vicinity of the period-two cusp. However, it appears that every harmonic family gives rise to a Cantor set of cusps. Because of our parameterization of the cubic map, period-one has no cusp but period-two contains one cusp and the two distinct branches of period-four contain two cusps, period-eight four cusps, and so on. Evidence for the Cantor set of doubly superstable orbits associated with these cusps for the quartic map has been discussed by Chang, Wortis, and Wright.[19] Such a structure appears to be generic for a large class of two-parameter maps. The study of the effects of external noise on the dynamics in these regions is obviously a complex and challenging task.

3. STOCHASTIC DIFFERENCE EQUATIONS: ESCAPE AND CONFINEMENT CRITERIA

The dynamics of the noise-driven cubic map is governed by the stochastic difference equation

$$x_{t+1} = C(x_t; a, b) + \eta_t \tag{3.1}$$

where the random variables η_t are identically distributed and belong to a

uniform rectangular distribution on the interval $[-\beta, \beta]$. Thus the probability density for any η_t is given by

$$W(\eta) = \begin{cases} (2\beta)^{-1} & \text{if } |\eta| \leqslant \beta \\ 0 & \text{otherwise} \end{cases} \tag{3.2}$$

This section is devoted to a description of the various escape, confinement, and transition criteria as β is changed involving noisy period-one and period-two orbits. We will show that in a transition, critical paths appear, which differentiate the ways in which probability flux may propagate within the system. The ensembles of critical paths governing these various fluxes determine the evolution of the density in the integral (field) representation of the system's dynamics, and are thereby closely related to the structure of this operator's spectrum and eigenstates, which are discussed in the following section.

The fact that the noise is amplitude limited leads to the possibility that there exist noisy periodic orbits with finite support.[10] Thus, we may examine the circumstances under which such bounded support exists, when several disjoint regions may merge, and when escape from the interval I is possible. It is simplest to consider first the antisymmetric cubic map ($b = 0$), and describe the processes that occur as β increases for various fixed values of a. We then turn to a brief discussion of the noisy dynamics for $b \neq 0$.

3.1. Period-One Regime

Recall that for the deterministic cubic map the origin is a stable period-one fixed point for $0 \leqslant a \leqslant 2$, $b = 0$. There are also unstable fixed points at ± 1. We examine first the noisy dynamics below superstability ($a < 1$). The map function in this region of parameter space is shown in Fig. 3a. The confinement and escape criteria for period-one are governed by the noise-limit (NL) map functions $C(x; a, b) \pm \beta$ (Fig. 3a). Iteration of a noisy map is similar to that for a deterministic map, except that the "noisy" image of a point always lies between the NL functions. Like the cubic map function itself, for small β these NL map functions also possess one stable and two unstable fixed points: $A_\pm$ are the stable fixed points of $C(x) \pm \beta$, while $B_\pm$ and $C_\pm$ are the unstable fixed points. From an examination of Fig. 3a it is clear that the stable fixed points $A_\pm$ determine the support of the noisy period one orbit: $\mathscr{S} = [A_-, A_+]$. The corresponding invariant density is shown in Fig. 3b.

The infinite interval $[-\infty, \infty]$ can be partitioned into several regions (see Fig. 3a) in which distinctive dynamics occur, and which provide a convenient reference for the discussion of the fate of iterates under the

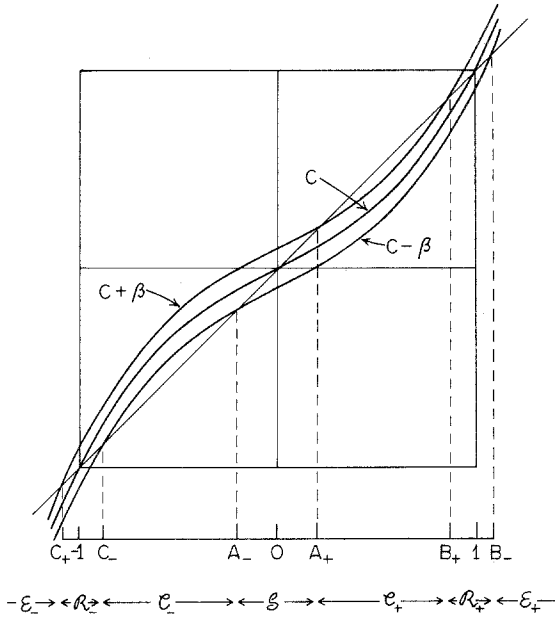

(a)

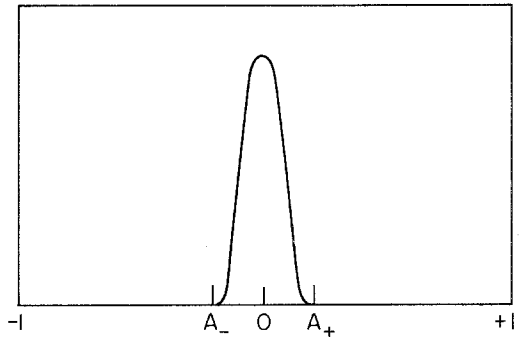

(b)

Fig. 3. (a) The cubic map (C) for $a = 0.5$ and $b = 0$. Also shown are the NL map functions $C(x; 0.5, 0) \pm \beta$ with $\beta = 0.1$. The fixed points of these functions are $A_\pm$, $B_\pm$ and $C_\pm$. The partition of the infinite interval $[-\infty, \infty]$ into the regions $\mathscr{S}$, $\mathscr{C}_\pm$, $\mathscr{R}_\pm$ and $\mathscr{E}_\pm$ discussed in the text is shown at the bottom of the figure. (b) The invariant density of the noisy map depicted in (a).

noisy map. Provided β is sufficiently small (see below), we may classify the dynamics in the various regions in the following way: (1) Points initially in $\mathscr{E}_\pm$ always escape to $\pm\infty$ and are never trapped; (2) points in the "reservoirs" $\mathscr{R}_\pm$ wander until they either are trapped by $\mathscr{E}_\pm$ and escape to $\pm\infty$ or enter the "channels" $\mathscr{C}_\pm$, in which case they eventually enter the asymptotic support $\mathscr{S}$ and are trapped. Thus, once points are in $\mathscr{S}$ they never leave it; points in $\mathscr{C}_\pm$ eventually end up in $\mathscr{S}$; points in $\mathscr{R}_\pm$ either enter $\mathscr{C}_\pm$ (and end up in $\mathscr{S}$) or enter $\mathscr{E}_\pm$ and escape.

The limits of the asymptotic support $\mathscr{S} = [A_-, A_+]$ are easily determined from the solutions of the fixed-point equations

$$C(A_\pm; a, 0) \pm \beta = A_\pm \tag{3.3}$$

which, for small values of β, are given approximately by $A_\pm = \pm\beta/a$, and therefore the support has measure $\mu(\mathscr{S}) = 2\beta/a$.

From an examination of Fig. 3a one may also see that the stable and unstable fixed-points in the pairs, (C_-, A_-) and (A_+, B_+), move toward each other as β increases, and finally coalesce at a critical value of $\beta = \beta_e$. For values of $\beta > \beta_e$ a stationary density no longer exists and iterates eventually escape to infinity. This escape mechanism involves a tangent bifurcation process for the NL map functions: at $\beta = \beta_e$ the slope of the NL map function at the marginally stable fixed points $A_\pm$ is unity $[C'(A_\pm) = 1]$; thus $A_\pm = \pm\sqrt{3}/3$, independent of a, and $C(A_\pm) \pm \beta_e = A_\pm$ yields $\beta_e = 2\sqrt{3}\,a/9$. When β increases beyond β_e the NL fixed points move into the complex plane and iterates may escape through the small channels that are formed, provided the proper noise sequence occurs: a long string of η_t values with $|\eta_t| \sim \beta$ is required for a passage through the channel. Thus, while escape is possible for $\beta \gtrsim \beta_e$, very long transients are to be expected for initial states with density in the central region. An almost successful passage through the channel is shown in Fig. 4. This figure also illustrates the iteration process for a stochastic sample path.

As a increases and deterministic period-one moves through superstability, new confinement and escape criteria must be applied. Although period one is stable for $a \leqslant 2$ we must apply separate escape criteria for $a < 4/3$ and $a > 4/3$. This value of a is a critical value for the antisymmetric cubic map where the minimum (maximum) is mapped under $C(x; a, 0) \pm \beta$ into the tangent fixed point of $C(x; a, 0) \pm \beta$, which, as noted earlier occurs at $x = \mp\sqrt{3}/3$:

$$C\left(\pm\left[\frac{a-1}{3a}\right]^{1/2}; a, 0\right) \mp \beta = C\left(\mp\frac{\sqrt{3}}{3}; a, 0\right) \mp \beta$$

which yields $a = 4/3$.

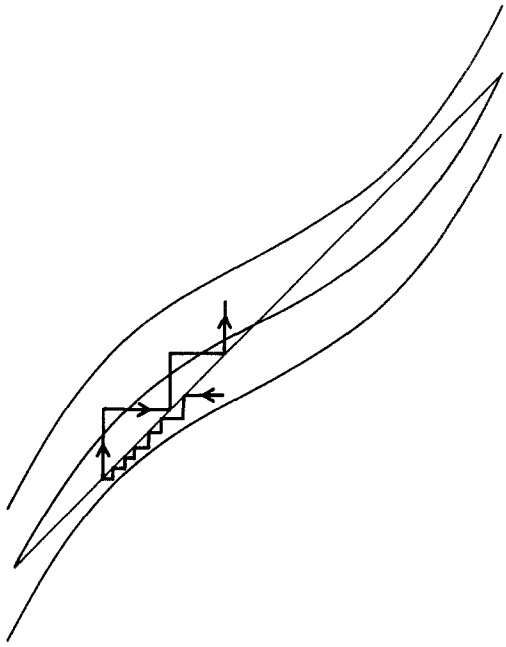

Fig. 4. A schematic representation of an almost successful passage through the channel which exists for the tangent escape mechanism.

Figure 5 is a sketch of the map for $1 < a < 4/3$, along with the associated NL functions $C(x) \pm \beta$ for two values of β. If β is sufficiently small it is possible to construct a stable, NL period-two orbit (shown in the center of the figure), which determines the asymptotic support of the noisy period-one orbit. More specifically, $\mathscr{S} = [L, R]$, where L and R are solutions of the fixed-point equations

$$C(L; a, 0) + \beta = R, \qquad C(R; a, 0) - \beta = L \tag{3.4}$$

Since the NL period-two orbit is stable, all noisy iterates of the map will be attracted to the interval $[L, R]$. For small β the NL period-two fixed points will lie near the origin and can be found from a linearized analysis: $R, L = \pm\beta/(2 - a)$. The NL period-one fixed points, $A_{\pm} = \pm\beta/a$, which are also solutions of Eq. (3.4), are shown in Fig. 5, along with R and L.

Increasing β causes the diameter of the NL period-two orbit to grow, and eventually its fixed points coincide with the maximum M and minimum m of the map. Since the extrema of the map are located at $M, m = \pm[(a - 1)/3a]^{1/2}$ the value of β at which this occurs, say, β_c, is easily

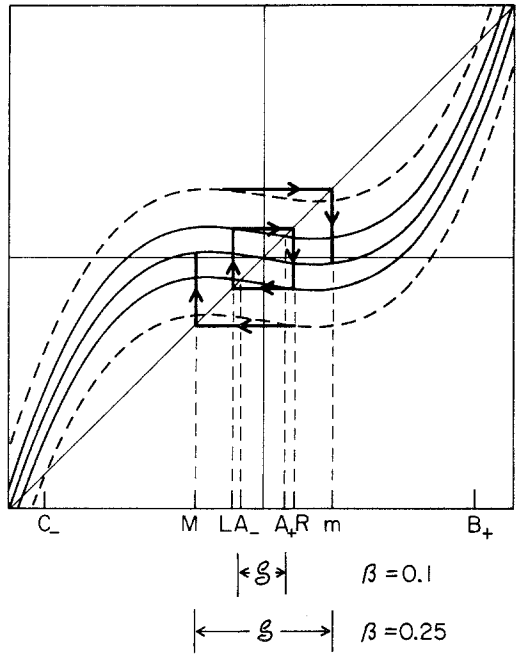

Fig. 5. The cubic map (center solid curve) for $a = 7/6$ and $b = 0$, along with the associated NL map functions for $\beta = 0.1$ (solid curves) and $\beta = 0.25$ (dashed curves). The relevant fixed points discussed in the text and the asymptotic support $\mathscr{S}$ are also shown.

found from the equation

$$C(M; a, 0) + \beta_c = m \tag{3.5}$$

and is given by

$$\beta_c = \frac{5 - 2a}{3}\left(\frac{a - 1}{3a}\right)^{1/2}$$

When $\beta > \beta_c$ the support of the noisy period-one orbit is determined by the noisy images of the maximum and minimum of the map: $\mathscr{S} = [C(m) - \beta, C(M) + \beta]$. This is also depicted in Fig. 5 for $\beta = 0.25$. This condition determines the asymptotic support until the NL map function becomes tangent to the bisectrix. The tangent escape mechanism discussed earlier then operates and iterates are no longer confined to a bounded region.

If $a < 4/3$ the minimum (maximum) is mapped to the right (left) of the tangent fixed point and the tangent mechanism determines the escape criterion. However, for $a > 4/3$ the reverse is true, and the minimum (maximum) is mapped under the NL map to the left (right) of the tangent

fixed point. As a result, escape will have occurred before tangency is reached and is now determined by the condition that the minimum (maximum) is mapped into the unstable fixed point C_- (B_+) (see Fig. 5),

$$C(m;a,0) - \beta = C_-$$

$$C(M;a,0) + \beta = B_+$$

In fact, this condition determines when escape occurs for $4/3 \leqslant a \leqslant 4$ regardless of the stable orbit supported by the deterministic map. We observe that this mechanism is an obvious analog of chaotic band breakdown; cf. Refs. 11 and 15.

3.2. Symmetric Period-Two Regime

In the absence of noise, period-two is born out of period-one by a pitchfork bifurcation at $a = 2$ ($b = 0$), and remains stable until $a = 3$, where a bifurcation into two distinct period-two orbits occurs. In the period-two region the support criteria are again most conveniently discussed in terms of NL map functions, except that one must now deal with NL functions for the second power of the map. We define these functions as

$$F^{\pm}(x;a,b,\beta) = \begin{cases} \max\limits_{-\beta \leqslant \eta \leqslant \beta} C\big[C(x) + \eta\big] + \beta \\ \min\limits_{-\beta \leqslant \eta \leqslant \beta} C\big[C(x) + \eta\big] - \beta \end{cases} \tag{3.6}$$

From the definition, Eq. (3.6), one can see that these functions represent the maximum excursion an iterate starting at x may take to the right (F^+) or left (F^-) in two iterations under C. In the vicinity of extrema of the map, values of $|\eta|$ which are smaller than β produce maximal excursions in two iterations of the map. An illustration of these second-power NL functions for a large value of β is shown in Fig. 2b. The flat regions of these functions correspond to $|\eta| < \beta$; they are much less pronounced for smaller β.

We first consider period-two just beyond marginal stability where $a \gtrsim 2$: here the orbit has a small diameter and is symmetric with respect to the origin for $b = 0$. In addition, in the relevant region the NL functions are simple and are given by

$$F^{\pm}(x;a,b,\beta) = C\big[C(x) \pm \beta\big] \pm \beta \tag{3.7}$$

A schematic diagram of the second power of the cubic map, $C^{(2)}(x;a,0)$, along with the NL functions $F^{\pm}$ is presented in Fig. 6 for small values of x. If we let $a = 2 + \epsilon$ with ϵ small, $C^{(2)}(x;a,0)$ possesses stable fixed

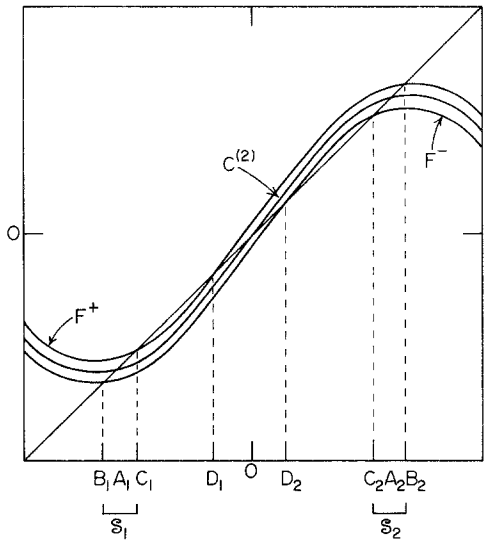

Fig. 6. A schematic diagram showing the shapes of the second power of the cubic map and the NL functions $F^{\pm}$ near the origin for $a \gtrsim 2$ and $b = 0$ when β is small. The fixed points and asymptotic supports are also indicated.

points at $A_{1,2} = \mp\sqrt{\epsilon}$ (the origin is an unstable fixed point); on the other hand, the NL function F^{+} (F^{-}) has stable fixed points at C_1 and B_2 (B_1 and C_2) and an unstable fixed point at D_1 (D_2). For small values of ϵ and β ($\beta/\epsilon \ll 1$) fixed points can be determined perturbatively and are given by

$$B_1, C_1 = -\sqrt{\epsilon} \mp \beta/2\epsilon$$

$$C_2, B_2 = -\sqrt{\epsilon} \mp \beta/2\epsilon$$

and

$$D_1, D_2 = \mp\beta/\epsilon$$

The situation is reminiscent of the period-one case depicted in Fig. 3a, except that the stability of the fixed points is interchanged. The disjoint support, $\mathcal{S}_{1,2}$, of the noisy period-two orbit is determined by the stable fixed points of $F^{\pm}$: $\mathcal{S}_1 = [B_1, C_1]$ and $\mathcal{S}_2 = [C_2, B_2]$. Using the above results for the fixed points, the measure of these supports for small values of ϵ and β are $\mu(\mathcal{S}_1) = \mu(\mathcal{S}_2) = \beta/\epsilon$. The densities in $\mathcal{S}_1$ and $\mathcal{S}_2$ are mapped cyclically into one another under the noisy cubic map.

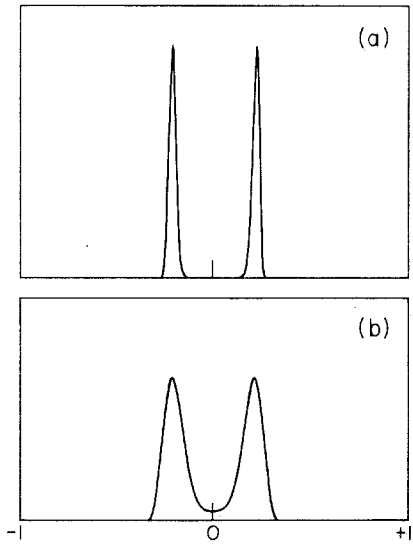

Fig. 7. (a) The invariant density for $a = 2.1 \gtrsim 2$ and $b = 0$ for $\beta = 0.02 < \beta_m$. (b) The invariant density for the same (a, b) values but $\beta = 0.05 > \beta_m$. The two disjoint bands have merged.

As β increases the fixed points C_1 and D_1 (D_2 and C_2) approach each other and coalesce at a critical value of $\beta = \beta_m$. (For small ϵ the critical condition $C_1 = D_1$ yields $\beta_m = (2/3)\epsilon^{3/2}$.) Beyond this value of β the disjoint noisy period-two components merge and a continuous invariant density exists between the (still stable) fixed points B_1 and B_2. The mechanism for the merging process is, of course, just the tangent mechanism described earlier. Figure 7 shows the invariant density just below β_m (two disjoint peaks) and above β_m where a bounded continuous density exists. When $a = 2.5$ ($b = 0$) the period-two orbit is doubly superstable, and it is clear that the merging mechanism changes. We shall not pursue the fate of noisy (singly stable) period-two in this paper, but instead discuss the bistable region.

3.3. Broken Symmetry Period-Two Regime

The analysis of the effects of small amounts of noise on the newly born ($a \gtrsim 3$) pair of the broken-symmetry period-two orbits is similar to that for the single period-two orbit which occurs by bifurcation from period-one. The second power of the map was shown in Fig. 2b for $a = 3.1$. At somewhat smaller values of a, locally, in the vicinity of the unstable

period-two fixed points, the map shape is similar to Fig. 6. Thus, the previous analysis applies directly to this case: one may again construct NL map functions $F^{\pm}$, whose stable fixed points determine the boundaries of the disjoint support of the components of the two distinct noisy period-two orbits. Again, as β is increased, a critical value of $\beta = \beta_2$ is reached where stable and unstable fixed points of $F^{\pm}$ (in the vicinity of the unstable period-two fixed points of the map) coalesce and the support is no longer disjoint: now a single noisy period-two orbit exists rather than two distinct period-two orbits. This was briefly described earlier in Ref. 13.

As a increases and the distinct period-two orbits move through superstability, new mechanisms are operative which are the analogs of the escape and confinement mechanisms for period-one for $a > 1$ (above superstability). This is depicted in Fig. 8, where a portion of the second power map near the period-two fixed point (cf. Fig. 2a) is shown. The support is determined by the noisy images under $F^{\pm}$ of the local extremum. For a certain range of a values, it is possible to map the local maximum M under F^{+} to the left of the unstable fixed point of F^{-}, D_2, before C_2 and D_2 coalesce and F^{-} is tangent to the bisectrix. The process is clearly similar to that described earlier for period-one. Note that the noisy iterates are no longer confined to a channel as in the tangent mechanism. For these values of a, one may also construct criteria for the merging of the resulting two

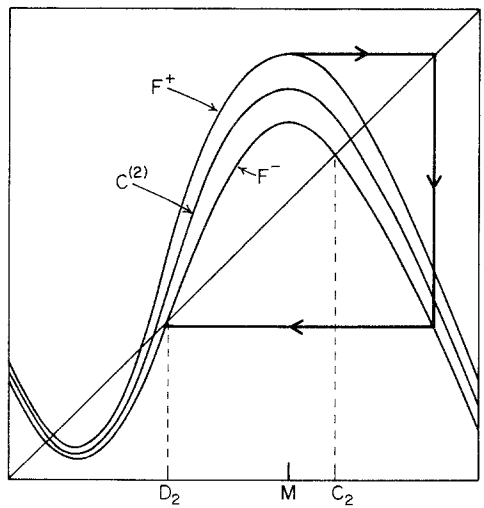

Fig. 8. Sketch of $C^{(2)}$ and $F^{\pm}$ near one (right, cf. Fig. 2a) of the unstable period-two fixed points. The figure shows how the local maximum M can be mapped to the left of D_2, leading to a merging of the two distinct noisy period-two orbits, before $F^{\pm}$ is tangent to the bisectrix.

disjoint supports and the consequent formation of a continuous invariant density.[13]

3.4. Noisy Dynamics for $b \neq 0$

We shall not give a detailed description of the processes that occur when the map is asymmetric, except to say that similar mechanisms to those described above again operate but, since $b \neq 0$, the processes are not symmetric with respect to the origin. Thus transitions may first occur from a particular period-two component rather than from both simultaneously.

The primary new feature that is introduced in going into the (a,b) plane, away from the line $b = 0$, is the possibility of studying the effects of noise on hysteresis phenomena. There are very interesting dynamics associated with the appearance and disappearance of the stable orbit as the tangent boundary t' (cf. Fig. 1b) is crossed. An illustration of these effects is presented in Fig. 9, which shows some of the processes that take place as b is tuned, at constant a, through the bistable region at various noise levels. In (a) a hysteresis loop is shown for the deterministic system: as one progresses from left to right the system first resides on the upper branch period-two orbit (only one component is shown) until, at a certain value of b, the right tangent boundary t' (Fig. 1b) is crossed and the system crashes to the lower branch period-two orbit. A similar process involving an upward transition occurs as b is tuned from right to left. The remaining figures (9b–d) show what happens to this hysteresis loop as increasing amounts of noise are added to the system. The figures were constructed by plotting the iterates of the noisy map, after most transient behavior is allowed to relax, for many different values of b. Thus, a cut through the figure at a particular b value gives the invariant density for the selected (a,b), and the given β value. [In some regions of the figure (4c), the system is not fully relaxed.] One observes processes in accord with merging criteria described earlier: in (b) we have two distinct noisy period-two orbits with crashes between these noisy orbits occurring at the ends of the hysteresis loop. Figure 4c shows the case where noise-induced transitions between the bistable orbits take place. The orbit components with disjoint support have merged and one has a single noisy period-two orbit. Each component of this period-two orbit has a density which is bimodal, as can be seen in the figure. In Figure 4d, which represents a still greater value of β, one can no longer distinguish the original period-two components; any vestige of the hysteresis loop has disappeared and one has a single noisy period-two orbit with unimodal density in its components.

Rather than elaborating on these interesting phenomena, we take up an integral equation description of noisy dynamical processes.

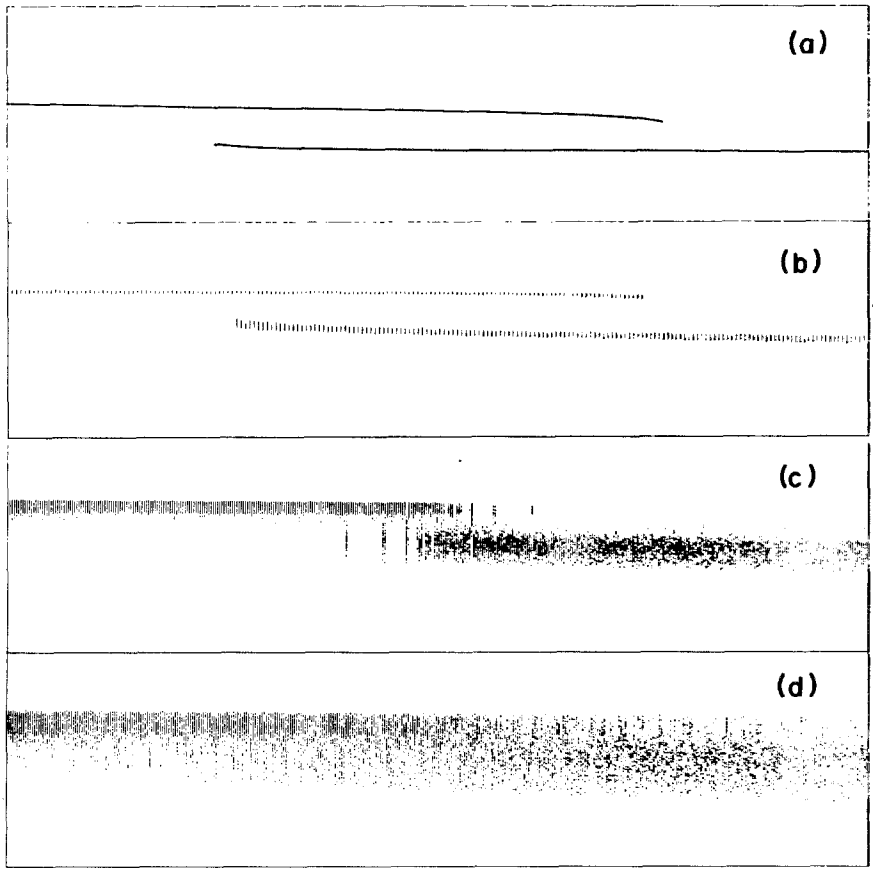

Fig. 9. Effects of noise on the hysteresis phenomena at $a = 3.1$ and varying b. (a) Deterministic map: $\beta = 0$, (b) noisy hysteresis loop $\beta = 0.005$, (c) transitions occur between the bistable states: $\beta = 0.025$, (d) bistable states can no longer be distinguished: $\beta = 0.100$.

4. INTEGRAL EQUATION DESCRIPTION

It is often convenient to describe relaxation processes in terms of the eigenvalue spectrum of an appropriate evolution operator for the system; the discrete dynamical system studied here has such a field representation. The discussion in Section 3, which was based on the stochastic (Langevin) difference equation, can be formulated in terms of a Chapman–Kolmogorov integral equation in order to obtain complementary information about the dynamics.[10,11,20]

From the stochastic difference equation (3.1) we see that the probability density for the random variable $x_{t+1} - C(x_t; a, b)$ is $W(\eta_t) \equiv W(\eta)$, and

so depends on β through Eq. (3.2). Thus, W is the transition probability density from x_t to x_{t+1}. Writing $x = x_{t+1}$ and $y = x_t$ the equation for the propagation of the density $\rho(x,t)$ may be written

$$\rho(x,t+1) = \int dy\, W[x - C(y;a,b)]\rho(y,t) \tag{4.1}$$

or more formally as

$$\rho(t+1) = \hat{W}\rho(t) \tag{4.2}$$

which defines the integral operator $\hat{W}$. Since $\hat{W}$ is not a symmetric operator it possesses distinct left and right eigenstates: the right eigenstates are physically more important since the probability density of the system may be expanded in terms of them, and we write the eigenvalue problem as

$$\hat{W}\rho_j = \lambda_j \rho_j \tag{4.3}$$

while the corresponding eigenvalue problem for the left eigenstates is

$$\phi_j \hat{W} = \lambda_j \phi_j \tag{4.4}$$

where $\hat{W}$ is understood to act to the left.

Before presenting results which are specific to the cubic map problem it is useful to give a brief general account of some of the spectral properties of Eq. (4.3). We note that

$$\int dx\, W(x,y) = 1 \tag{4.5}$$

that is, probability is conserved by $\hat{W}$. This leads to a number of conditions on the spectrum. Some of these have been given earlier by Chang and Wright.[11] The spectrum of such an operator lies in the closed unit disk in the complex λ plane. Any equilibrium state belongs to the eigenvalue $\lambda = 1$, the degeneracy of this eigenvalue being the number of distinct equilibria under $\hat{W}$. There may also be a periodicity underlying the equilibrium, as in the case of the noisy period-two state. All equilibrium states of this kind have associated eigenstates with unimodular eigenvalues ($|\lambda| = 1$); their existence prevents strict relaxation to the equilibrium.[11] However, all suitable initial states relax to a linear combination of these "unimodular" states.

In numerical computations employing Eq. (4.1) the continuous space Markov process was approximated by a sufficiently fine discrete Markov process in the space coordinate. The condition, Eq. (4.5), shows that $\hat{W}$ is just the continuous analog of a transposed stochastic matrix. The Frobenius–Perron theorem[21] predicts the properties of both the eigenfunctions and spectra of such stochastic matrices. In particular, if $\mathcal{S}_1$, $\mathcal{S}_2, \ldots, \mathcal{S}_n$ is an invariant sequence of disjoint sets visited cyclically

($\mathcal{S}_j \to \mathcal{S}_{j+1}$, $\mathcal{S}_n \to \mathcal{S}_1$) then the entire spectrum of the eigenstates, whose support is the union $\mathcal{S} = \bigcup_j \mathcal{S}_j$, of this sequence is cyclic. Thus for period-two (with two components for $\mathcal{S}$) both λ and $-\lambda$ belong to the spectrum. It is easily shown that if λ is a complex eigenvalue of $\hat{W}$, $\bar{\lambda}$ is also an eigenvalue. Thus for period-two, on $\mathcal{S}$, the spectrum may in general contain quartets of eigenvalues $\{\lambda, -\lambda, \bar{\lambda}, -\bar{\lambda}\}$ which have simply related eigenstates. These results refer only to the asymptotic support $\mathcal{S}$ and are not true for states that extend outside $\mathcal{S}$. This property has been noted earlier for the unimodular spectrum[11] and the above remarks show that it holds more generally and illustrates the close connection between the structure of $\mathcal{S}$ and the spectrum of $\hat{W}$ restricted to $\mathcal{S}$. As implied earlier the cyclic character of the spectrum is a manifestation of the phase-coherent, periodic nature of the associated set of states. We shall present examples of phenomena involving such cyclic states as the amplitude of the external noise varies.

Another feature of the class of integral operators discussed here is that with respect to the asymptotic support $\mathcal{S}$ the integral operator $\hat{W}$ is completely continuous and therefore zero is the only accumulation point of its spectrum.[22]

We now turn to a discussion of the spectral properties of the noisy cubic map in the period-one and period-two regimes. In the course of this discussion we shall present the results of numerical solutions of Eq. (4.1) obtained by taking a finite grid for the space variable. It is, of course, clear that one must be careful that the grid size in any such simulation of the continuous space Markov process is finer than the scale of the phenomenon one is investigating.

4.1. Period-One Regime

It was noted in the previous section that provided $\beta < \beta_e$ noisy period-one orbits with finite support $\mathcal{S}$ could be obtained for $0 \lesssim a \lesssim 2$. We again initially focus our attention on the antisymmetric cubic map for simplicity. We shall first consider the character of the eigenvalue spectrum of the states (equilibrium and relaxing) defined on this support as the map parameter a varies. The equilibrium state $\rho_1(x)$ (belonging to the eigenvalue $\lambda_1 = 1$) is nondegenerate; we examine the structure of the slowest relaxing state.

The major gross feature that is observed is the change in character of the relaxing eigenvalues as the map parameter passes through superstability, $a = 1$: for the deterministic map below superstability one observes monotone convergence to the period-one fixed point, while above superstability there is alternating convergence. This feature is reflected in the

eigenvalue of the slowest relaxing state: it is positive below superstability and negative above. If one considers the evolution of an arbitrary initial state defined on $\mathscr{S}$, $\rho_s(x)$, then this state can be expanded in terms of the (complete) set of eigenstates of $\hat{W}$ with support $\mathscr{S}$,

$$\begin{aligned} \rho_s(x) &= \sum_j a_j \rho_j(x) \\ a_j &= \int_{\mathscr{S}} dx\, \phi_j(x) \rho_s(x) \end{aligned} \tag{4.6}$$

Thus for long times

$$\rho_s(x,t) = a_1 \rho_1(x) + \lambda_2^t a_2 \rho_2(x) \tag{4.7}$$

where we have taken $\rho_2(x)$ to be the slowest relaxing state; one sees the change in character of the time evolution of the initial density as a passes through superstability because of the change of sign of λ_2.

In the vicinity of the superstable point one may examine the solutions of the integral master equation in more detail if the noise amplitude is small. Since the origin is the period-one fixed point of the deterministic system small amounts of noise will produce noisy orbits with support with small measure $\mathscr{O}(\beta)$ centered about the origin (see Section 3). If we let $a = 1 - \epsilon$, with ϵ a small parameter, we may then expand the integral kernel $W[x - C(y; a, 0)]$ as

$$W\big[x - C(y; a, 0)\big] = W(x) - \epsilon W'(x) y - (1 - \epsilon) W' y^3 + \mathscr{O}(\epsilon^2) \tag{4.8}$$

The equilibrium eigenvector $\rho_1(x)$, which is symmetric about the origin due to the map symmetry, corresponds to the eigenvalue $\lambda_1 = 1$; we have [Eq. (4.3)]

$$\rho_1(x) = \int_{\mathscr{S}} dy\, W\big[x - C(y; a, 0)\big] \rho_1(y) = W(x) + \mathscr{O}(\epsilon^2) \tag{4.9}$$

where the higher-order terms from Eq. (4.8) vanish by symmetry and the fact that the equilibrium state is normalized as $\int_{\mathscr{S}} \rho_1(x)\, dx = 1$ has been used. Thus near superstability ($\epsilon = 0$) the equilibrium state is given by the probability distribution for the noise. This is borne out by the results in Fig. 10a which clearly show that the equilibrium density has a roughly rectangular distribution. Using Eq. (4.8) for the integral kernel one may also compute the slowest relaxing state (with support $\mathscr{S}$). To order ϵ the eigenvalue problem reads

$$\lambda_2 \rho_2(x) = -\big[\epsilon \nu_1 + (1 - \epsilon)\nu_3\big] W'(x) \tag{4.10}$$

where

$$\nu_n = \int_{\mathscr{S}} dy\, y^n \rho_2(y) \tag{4.11}$$

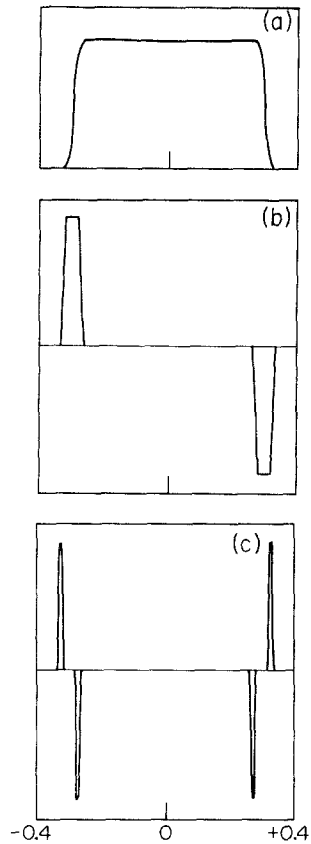

Fig. 10. (a) The invariant density near superstability: $a = 1.0$; $b = 0$, $\beta = 0.3$. The approximately rectangular distribution of the equilibrium density is clearly evident. (b) Antisymmetric relaxing eigenvector for the same conditions. (c) Symmetric relaxing eigenvector for same conditions.

It follows after a suitable selection of normalization) that

$$\rho_2(x) = W'(x) \tag{4.12}$$

and

$$\lambda_2 = \epsilon + (1 - \epsilon)\beta^2 \tag{4.13}$$

The above analysis predicts that the relaxing eigenvalue should be a linear function of β^2 with intercept ϵ near superstability and for small β. Numerical results for λ_2 are presented in Fig. 11 for two values of $\epsilon = \pm 0.1$ as a function of β^2. All relaxation eigenvalues were estimated by the power

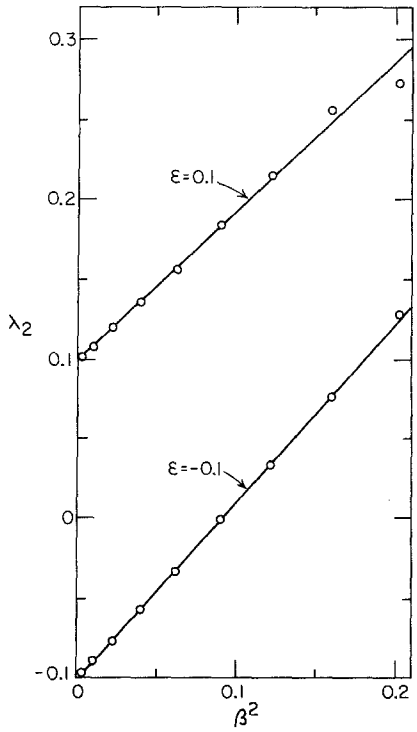

Fig. 11. Plot of the slowest relaxing eigenvalue with support $\mathscr{S}$ as a function of β^2 for two values of ϵ: upper curve, $\epsilon = 0.1$, below superstability, the slope is 0.945 (predicted 0.9); lower curve, $\epsilon = -0.1$, above superstability, the slope is 1.125 (predicted 1.1). The relaxing state is antisymmetric.

method (iteration) after projecting out the equilibrium state by subtraction. The linear variation of λ_2 with β^2 is confirmed as is the value of λ_2 at $\beta = 0$. In addition, the predicted slope, $1 - \epsilon$, is in rough accord with the numerical values. As a further test one may examine the behavior of the relaxing eigenvalue and superstability. Equation (4.13) implies $\lambda_2(\epsilon = 0) = \beta^2$, which is confirmed by the estimated slope of 2.05 in Fig. 12. The relaxation near superstability is very fast. The expression for the (antisymmetric) relaxing eigenvector in Eq. (4.12), which may be written as

$$\rho_2(x) = (2\beta)^{-1}[\delta(x + \beta) - \delta(x - \beta)] \tag{4.14}$$

implies that for $\epsilon \cong 0$ this eigenvector should be flat and nearly zero in the center of the support and sharply peaked at the ends. Figure 10b confirms this structure. This analysis can be extended one step further to predict a

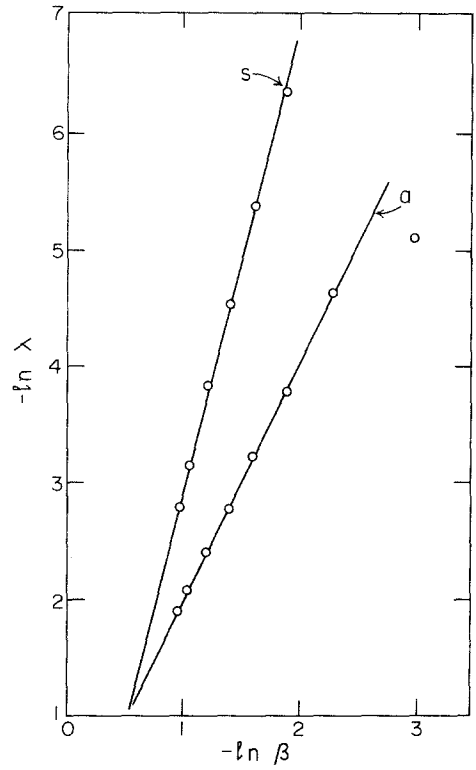

Fig. 12. Plot of relaxation eigenvalues $-\ln\lambda_2$ (a) and $-\ln\lambda_3$ (s) versus $-\ln\beta$ at superstability ($a = 1.0$, $b = 0$). The computed slope for the antisymmetric state (a) is 2.05 corresponding to the prediction $\lambda_2 = \beta^2$ and the slope for the symmetric state (s) is 4.13 corresponding to $\lambda_3 = 3\beta^4$ (cf. Fig. 10).

(right) symmetric relaxing state proportional to $\delta'(x+\beta) + \delta'(x-\beta)$ belonging to the eigenvalue $\lambda_3 = 3\beta^4$. Again careful numerical work confirms this prediction very well: the calculated β exponent of λ_3 is 4.13 (see Fig. 12) and Fig. 10c shows the appearance of the computed eigenvector. [Formally one may continue this procedure but the singular structure of the (right) eigenvectors prevents easy computation of higher states.]

In obtaining the results presented in Figs. 10–12 care was taken to insure that the initial states were within a specified interval (see below) containing the asymptotic support. However, arbitrarily prepared initial states may have components from eigenstates with support outside of $\mathscr{S}$: such eigenstates may relax more slowly than those with support $\mathscr{S}$ and, as a consequence, they will govern the long-time behavior of the system. The manner in which this occurs can be described by referring to the partition

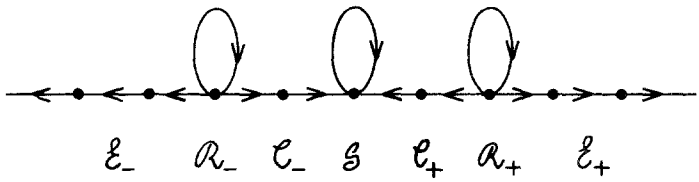

Fig. 13. Digraph for the Markov chain model exhibiting features of the relaxing states with support outside $\mathscr{S}$. Regions of escape $\mathscr{E}_\pm$ are represented by strings of vertices; the channels $\mathscr{C}_\pm$ connecting the reservoirs $\mathscr{R}_\pm$ to the support $\mathscr{S}$ are represented by single vertices. Vertices without loops correspond to one-way flux.

of the infinite interval $[-\infty, \infty]$ given in the inset of Fig. 3a, and the discussion of the dynamics on this partition in Section 3. Recall that initial states in the reservoirs $\mathscr{R}_\pm$ may either enter $\mathscr{E}_\pm$ and escape or enter $\mathscr{C}_\pm$ and thus ultimately become trapped in $\mathscr{S}$. The dynamics can be crudely modeled and discussed in terms of the Markov chain in Fig. 13. Like the Chapman–Kolmogorov equation, this Markov chain possesses an equilibrium eigenvector associated with the state $\mathscr{S}$, reservoir states $\mathscr{R}_\pm$ from which transitions may occur to channels $\mathscr{C}_\pm$ and to (the infinite number of)

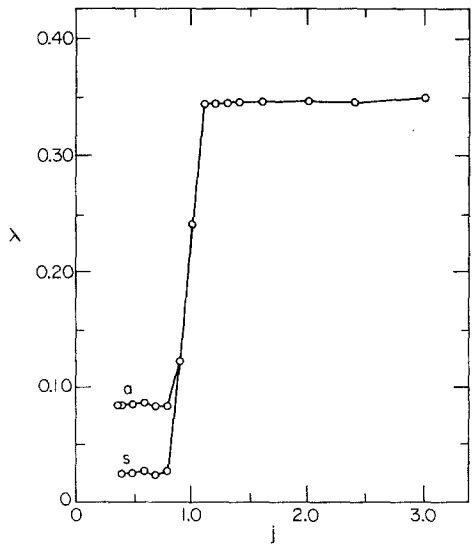

Fig. 14. Estimate of relaxation eigenvalue λ at superstability ($a = 1.0$, $b = 0$) and $\beta = 0.3$ as function of integration interval $J = [-j, j]$ starting from antisymmetric state (a) and symmetric state (s). If $J \supset \mathscr{R}_+ \cup \mathscr{R}_-$ the (a) and (s) λ values coincide. For $J \not\supset \mathscr{R}_\pm$ with (a) and (s) λ values correspond to the support $\mathscr{S}$.

states in $\mathscr{E}_{\pm}$ where there is a one-way current. For such a Markov chain it is easy to verify that the system need not have a complete set of eigenstates, and states that relax into the equilibrium state need not be normalizable. Numerical simulations of the integral equation have verified the existence of relaxing states with such properties. Figure 14 shows the estimated relaxation eigenvalue λ_J for varying integration interval $J = [-j, j]$ at constant noise amplitude $\beta = 0.3$ and $a = 1$, $b = 0$. If J contains the reservoirs $\mathscr{R}_{\pm}$, λ_J (estimated iteratively) is large and independent of the symmetry of the initial state: λ_J depends only on the equal, forward transition rates out of the reservoirs. As the end points of J move inward through the reservoirs λ_J decreases rapidly since the probability of remaining in the remnant of $\mathscr{R}_{\pm}$ in J decreases. If J contains no part of $\mathscr{R}_{\pm}$ the symmetry of the initial state determines whether λ_J assumes the (small) symmetric or antisymmetric relaxation value on $\mathscr{S}$; the channels do not contribute since, under iteration, the one-way flux in $\mathscr{E}_{\pm}$ sweeps any amplitude into $\mathscr{S}$. If $b \neq 0$ $\mathscr{R}_{\pm}$ are no longer equivalent and relaxation occurs at a different rate from each reservoir.

4.2. Period-Two Regime

We shall now give a brief account of some features of the eigenvalue spectrum for values of the map parameter where the deterministic system supports period-two orbits. The emphasis of the discussion will be on the change in character of the eigenvalue spectrum as the noise amplitude is tuned through the various critical values defined in Section 3, and on the dependence of the relaxing states on the noise amplitude.

As an example we suppose that the deterministic system is in the bistable region and two period-two orbits coexist. (The specific results presented below are for $a = 3.1$ and $b = 0$.) As noted earlier, if the external noise amplitude is small, $\beta < \beta_2$, the asymptotic support consists of four disjoint bands, $\mathscr{S} = \bigcup_{i=1}^{4} \mathscr{S}_i$. These distinct noisy bands are visited cyclically in pairs, corresponding to the existence of two noisy period-two orbits: $\mathscr{S}_1 \to \mathscr{S}_3 \to \mathscr{S}_1$ and $\mathscr{S}_2 \to \mathscr{S}_4 \to \mathscr{S}_2$. Hence, in accord with our general discussion there are eigenvectors defined on $\mathscr{S}$ with eigenvalues $\lambda = \pm 1$, each of which is doubly degenerate. As β increases beyond β_2 a bifurcation (described by the mechanisms in Section 2) occurs in which transitions between the two noisy period-two orbits take place. Thus the supports $\mathscr{S}_1$ and $\mathscr{S}_2$ are joined into a single support $\mathscr{S}_1'$, as are $\mathscr{S}_3$ and $\mathscr{S}_4$ to form $\mathscr{S}_2'$. Close to β_2 the density is strongly peaked near the components of the previously stable noisy period-two orbits (see also Fig. 9c). This transition entails the lifting of the degeneracy of the eigenvectors associated with $\lambda = \pm 1$, but phase coherence is preserved since $\mathscr{S}_1'$ and $\mathscr{S}_2'$ are still

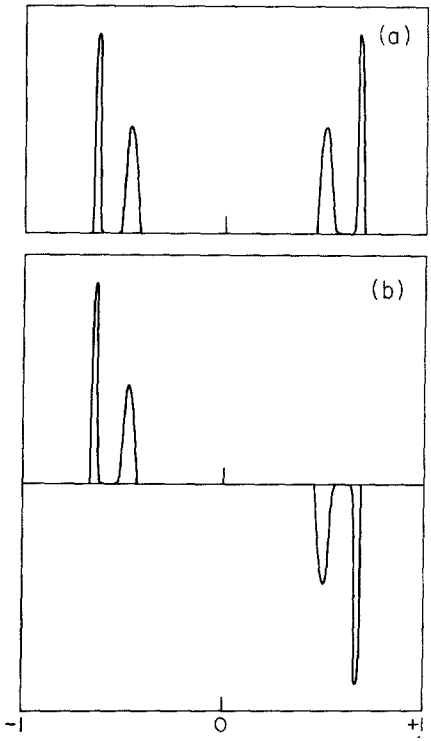

Fig. 15. (a) Eigenstate corresponding to $\lambda = 1$: $a = 3.1$, $b = 0$, $\beta = 0.015$. (b) Eigenstate corresponding to $\lambda = -1$ for the same parameter values.

mapped cyclically into one another, $\mathscr{S}_1' \to \mathscr{S}_2' \to \mathscr{S}_1'$. Thus, just beyond the transition the (now nondegenerate) $\lambda = \pm 1$ eigenvalues persist and there exist two relaxing eigenvalues $\pm\lambda$ with $|\lambda| \lesssim 1$. The eigenvectors corresponding to $\lambda = \pm 1$ are shown in Fig. 15 for $2\beta = 0.03$. We note that if $\beta < \beta_2$ and four disjoint supports exist, symmetric and antisymmetric eigenfunctions can be constructed corresponding to the eigenvalues $\lambda = \pm 1$: let $\gamma(x)$ be the equilibrium density on $\mathscr{S}_1$ ($\mathscr{S}_4$) and $\mu(x)$ that on $\mathscr{S}_2$ ($\mathscr{S}_3$), then clearly $\hat{W}(\gamma + \mu) = (\gamma + \mu)$ and $\hat{W}(\gamma - \mu) = -(\gamma - \mu)$ since $\hat{W}\gamma = \mu$ and $\hat{W}\mu = \gamma$. This character is also observed in the results in Fig. 15. The behavior of the eigenvalue corresponding to the symmetric relaxing state with $\lambda \gtrsim -1$ is shown in Fig. 16 as a function of the noise amplitude. From this figure it can be seen that λ approaches -1 very slowly as β goes to β_2 ($\beta_2 = 0.00691301$ for $a = 3.1$, $b = 0$)[13]; this is a reflection of the "softness" of the transition, which is expected in view of the mechanisms

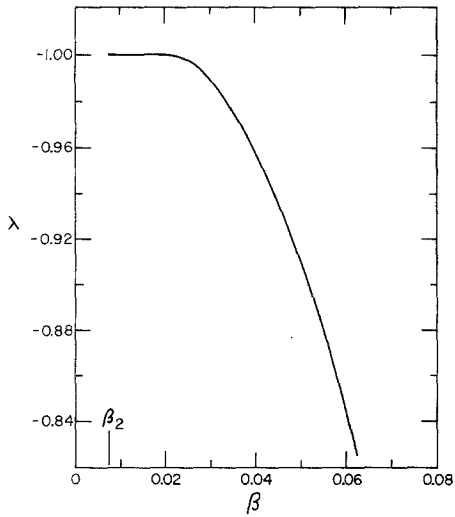

Fig. 16. Dependence of λ on β for the symmetric relaxing state with negative eigenvalue: $a = 3.1$, $b = 0$. β_2 is the critical β value for merging of distinct noisy period-two orbits.

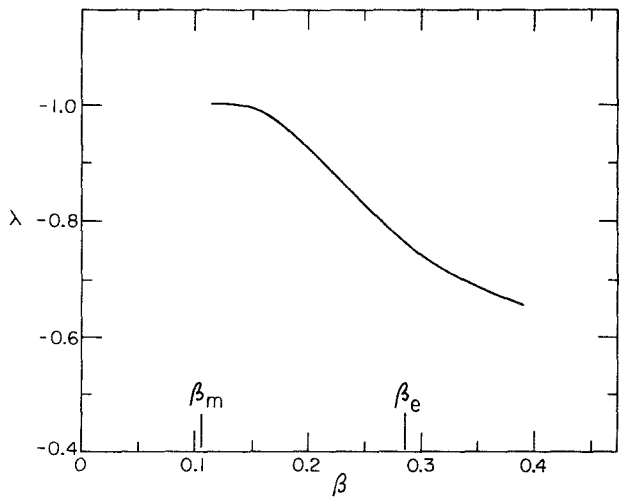

Fig. 17. Dependence of λ on β for the antisymmetric relaxing "gap" state: $a = 3.1$, $b = 0$. β_m marks critical β value for joining of support from two disjoint regions into one connected region by filling the central gap. β_e marks β value for escape. No invariant density on bounded support exists above β_e.

responsible for transition process (cf Section 3): the density in the region between the components increases smoothly although the support changes discontinously.

The next transition that occurs as β increases is the joining of the disjoint supports $\mathscr{S}_1'$ and $\mathscr{S}_2'$ to form an equilibrium state with a continuous invariant density. This occurs at $\beta = \beta_m$. As β increases beyond β_m phase coherence is lost and $\lambda = -1$ is no longer an eigenvalue of $\hat{W}$. Once again, although the transition is abrupt, the density between the noisy period-two peaks changes smoothly; this is again reflected in the behavior of the eigenvalue corresponding to this antisymmetric "gap" state; it approaches $\lambda = -1$ smoothly as β goes to β_m ($\beta_m = 0.10457772$ for $a = 3.1$, $b = 0$)[13] (cf. Fig. 17).

We have not attempted to construct models for the β dependence of these relaxation eigenvalues as β approaches the critical values of β_2 or β_m, although this could be done on the basis of the mechanisms presented in Section 3.

To complete the picture of the changes that occur as β increases we note that when β surpasses β_e, the escape value, $\lambda = 1$ is no longer an eigenvalue and slowly relaxing states associated with this transition appear (see Fig. 17).

5. CONCLUSION

We have presented two complementary descriptions of noise-induced transition and relaxation phenomena for the cubic map. From a consideration of the dynamics in terms of the stochastic cubic map, mechanisms for the various transitions that take place when the map parameters and noise amplitude are varied were presented. These same processes were then related to the spectral properties of the integral operator in the Chapman–Kolmogorov equation. In this paper we have focused on the behavior in the period-one and period-two regions of the map. Even here the rather large number of processes that take place required detailed study. However, it is seen that these noise-induced phenomena can be described in terms of a few mechanisms, for example, the tangent mechanism below superstability and the analog of chaotic band breakdown[11,15] above superstability. For the bounded-noise-amplitude case studied here the supports of the various noisy orbits change abruptly but the transitions appear smooth since the density between such noisy bands increases smoothly from zero. This is reflected in the behavior of the eigenvalues corresponding to relaxing states near the transitions: they appear to approach these limiting values smoothly as the noise amplitude approaches the transition value.

Although most of the results presented in the paper apply to the antisymmetric cubic map ($b = 0$), one of the primary motivations for our investigation of the noisy dynamics of the cubic map is the fact that the effects of noise on hysteresis phenomena can be studied by considering the map in the (a, b) plane. The effects that are observed as the noise amplitude is increased, such as a shrinking of the hysteresis loop and enhanced stability of stable states, are similar to those observed in stochastic differential equations.[1] The system is especially susceptible in the cusp region and near the tangent boundaries where "crashes" between bistable states occur in the deterministic system. The investigation of the dynamics of such processes is an interesting topic. The connection between the deterministic dynamics of flows exhibiting hysteresis and the corresponding phenomena in the map has been noted[4]; however, no detailed studies of the nature of the noisy map corresponding to a noisy flow have been reported. We are currently investigating this problem in connection with the cubic map as a model of the Rösler equations. In some circumstances it is possible to construct one-dimensional models for real systems where certain map parameters are directly related to physical control parameters.[6,17] The present investigation of noisy maps should be directly applicable to the analysis of such systems when the control parameters are subject to fluctuations.

The amplitude-limited noise case studied here is rather special: it permits the existence of noisy dynamics on intervals with bounded support. This behavior should be contrasted with that of unbounded noise sources, such as Gaussian noise. Here escape to infinity is always possible and a stationary equilibrium density cannot be established. In spite of this difference the mechanisms constructed for the amplitude-limited-noise case may also be of some use in the analysis of the effects of unbounded noise. We saw that although the support changed discontinuously for bounded noise the onset of transitions was actually smooth. For unbounded noise the supports are always joined, but transitions may only occur rarely for low RMS noise amplitudes, and only readily when certain conditions on the RMS amplitudes, similar to those in the mechanisms described above, are satisfied.

The present study provides a framework for studies of transition and relaxation processes that occur in noisy one-dimensional maps.

ACKNOWLEDGMENTS

This research was supported in part by the Natural Sciences and Engineering Research Council of Canada.

REFERENCES

1. L. Arnold and R. Lefever, eds., *Stochastic Nonlinear Systems in Physics, Chemistry and Biology*, (Springer Verlag, New York, 1981); G. Nicolis and I. Prigogine, *Self Organization in Nonequilibrium Systems* (Wiley, New York, 1977).
2. P. Collet and J.-P. Eckmann, *Iterated Maps on the Interval as Dynamical Systems* (Birkhäuser, Boston, 1980); R. Shaw, *Z. Naturforsch* **A36**:80 (1981); E. Ott, *Rev. Mod. Phys.* **53**:655 (1981); R. H. G. Helleman, in *Fundamental Problems in Statistical Mechanics*, Vol. 5, E. G. D. Cohen, ed. (North-Holland, New York, 1980), p. 165.
3. O. Rössler, *Ann. N.Y. Acad. Sci.* **316**:376 (1979).
4. S. Fraser and R. Kapral, *Phys. Rev. A* **25**:3223 (1982).
5. C. Tresser, C. Coullet, and A. Arneodo, *J. Phys. Lett.* **41**:2243 (1980).
6. J.-C. Roux, Experimental studies of bifurcations leading to chaos in the Belousof–Zhabotinsky reaction, *Physica D*, to be published.
7. A. C. Fowler and M. J. McGuinness, *Phys. Lett.* **92A**:103 (1982).
8. J. V. Noble, *Bull. Am. Phys. Soc.* **21**:371 (1976).
9. J. P. Crutchfield, J. D. Farmer, and B. A. Huberman, *Phys. Repts.* **92**:45 (1982).
10. G. Mayer-Kress and H. Haken, *J. Stat. Phys.* **26**:149 (1981); G. Mayer-Kress and H. Haken, Attractors of convex maps with positive Schwartzian derivative in the presence of noise, to be published.
11. S.-J. Chang and J. Wright, *Phys. Rev. A* **23**:1419 (1981).
12. B. A. Huberman and J. B. Crutchfield, *Phys. Rev. Lett.* **43**:1743 (1979); R. Kapral, M. Schell, and S. Fraser, *J. Phys. Chem.* **86**:2205 (1982); P. Mandel and T. Erneux, *Optica Acta* **29**:7 (1982); O. Decroly and A. Goldbeter, *Proc. Natl. Acad. Sci. U.S.A.*, **79**:6917 (1982); A. C. Fowler and M. J. McGuiness, *Phys. Lett.* **92A**:103 (1982).
13. E. Celarier, S. Fraser, and R. Kapral, *Phys. Lett.* **94A**:247 (1983).
14. R. May, *Ann. N.Y. Acad. Sci.* **316**:517 (1979).
15. M. Schell, S. Fraser, and R. Kapral, *Phys. Rev. A* **26**:504 (1982).
16. S. Grossman and H. Fujisaka, *Phys. Rev. A* **26**:1779 (1982).
17. L. Glass and R. Perez, *Phys. Rev. Lett.* **48**:1772 (1982); R. Perez and L. Glass, *Phys. Lett.* **90A**:441 (1982); M. Schell, S. Fraser and R. Kapral, *Phys. Rev. A* **28**:373 (1983).
18. J. Testa and G. A. Held, Period doubling, bifurcations, chaos, and periodic windows of the cubic map, preprint (1982).
19. S.-J. Chang, M. Wortis and J. A. Wright, *Phys. Rev. A* **24**:2669 (1981).
20. Y. Oono and Y. Takahaski, *Prog. Theor. Phys.* **63**:1804 (1980); H. Haken and G. Mayer-Kress, *Phys. Lett.* **84A**:159 (1981); H. Fujisaka and T. Yamada, *Z. Naturforsch*, **33a**:1455 (1978); H. Mori, B.-C. So, and T. Ose, *Prog. Theor. Phys.* **66**:1266 (1981); S. Grossmann and S. Thomae, *Z. Naturforsch.* **32a**:1353 (1977); H. Haken and A. Wunderlin, *Z. Phys. B*, 181 (1982).
21. D. R. Cox and H. D. Miller, *The Theory of Stochastic Processes* (Chapman and Hall, New York, 1965); F. R. Gantmacher, *The Theory of Matrices*, Vol. II (Chelsea, New York, 1974).
22. N. I. Akheizer and I. M. Glazman, *Theory of Linear Operators in Hilbert Space*, Vol. 1 (Ungar, New York, 1966).